

Article

Coexisting Attractor in a Gyrostat Chaotic System via Basin of Attraction and Synchronization of Two Nonidentical Mechanical Systems

Muhammad Marwan ^{1,*} , Vagner Dos Santos ^{2,3} , Muhammad Zainul Abidin ^{1,*}  and Anda Xiong ⁴¹ College of Mathematics and Computer Science, Zhejiang Normal University, Jinhua 321004, China² Department of Mathematics and Statistics, State University of Ponta Grossa, Ponta Grossa 84030-900, Paraná, Brazil; vagdsantos@gmail.com³ Universitário Faculdade de Telémaco Borba UNIFATEB, Telémaco Borba 84266-010, Paraná, Brazil⁴ School of Physics and Astronomy, University of Birmingham, Birmingham B15 2TT, UK; axx884@student.bham.ac.uk

* Correspondence: marwan78642@zjnu.edu.cn (M.M.); mzainulabidin@zjnu.edu.cn (M.Z.A.)

Abstract: This paper is divided into two main portions. First, we look at basins of attraction as a tool with a unique set of characteristics for discussing multistability and coexisting attractors in a gyrostat chaotic system. For the validation of coexisting attractors in different basins, several approaches such as bifurcation diagrams, Lyapunov exponents, and the Poincaré section are applied. The second half of the study synchronizes two mechanical chaotic systems using a novel controller, with gyrostat and quadrotor unmanned aerial vehicle (QUAV) chaotic systems acting as master and slave systems, respectively. The error dynamical system and the parameter updated law are built using Lyapunov's theory, and it is discovered that under certain parametric conditions, the trajectories of the QUAV chaotic system overlap and begin to match the features of the gyrostat chaotic system.

Keywords: nonlinear dynamical systems; basin of attraction; chaos; coexisting attractor; synchronization

MSC: 34C28; 34C60; 37N05; 34D06; 37D10



Citation: Marwan, M.; Dos Santos, V.; Abidin, M.Z.; Xiong, A. Coexisting Attractor in a Gyrostat Chaotic System via Basin of Attraction and Synchronization of Two Nonidentical Mechanical Systems. *Mathematics* **2022**, *10*, 1914. <https://doi.org/10.3390/math10111914>

Academic Editors: João Cabral, Daniele Fournier-Prunaret and José Leonel Linhares da Rocha

Received: 7 May 2022

Accepted: 31 May 2022

Published: 2 June 2022

Publisher's Note: MDPI stays neutral with regard to jurisdictional claims in published maps and institutional affiliations.



Copyright: © 2022 by the authors. Licensee MDPI, Basel, Switzerland. This article is an open access article distributed under the terms and conditions of the Creative Commons Attribution (CC BY) license (<https://creativecommons.org/licenses/by/4.0/>).

1. Introduction

Attracting the attention of many researchers since its first use for the investigation of earth rotation in 1852, the gyrostat has been used in a great variety of physical objects, such as QUAV, motor vehicles, spacecrafts, robots and so on. Moreover, industries that are dependent upon the positioning and movement of objects through robots can also use a gyrostat for stability [1]. Jalili and Emami [2] worked on finding the analytical solutions of industrial machinery in turning processing, while Pivarčiová et al. analyzed a mobile robotic system through an inertial navigation system [3]. In 2016, the combination of a tractor–trolley–trailer system [4] was modeled to provide mobility for the passage of a circular traffic jam. Chaos is an important phenomenon, which is famous for its sensitivity to initial conditions and parameter values. Apart from famous chaotic systems such as the weather forecast [5], finance [6] and biological [7] models, chaos in mechanical systems is demanding discussion in this technological era. In 2012, Aslanov and Yudintsev [8] considered a free gyrostat with small asymmetrical rotors and used an advanced Melnikov function to determine homoclinic and heteroclinic orbits in a controlled manner. In 2001, Kuang et al. [9] used Depri't variable for the first time to investigate chaos in the attitude motion of a gyrostat satellite. A mathematical model for the orbital motion of the attitude dynamics of a gyrostat attached to a satellite was derived by Abtahi [10], whereas Qi et al. [11] modeled a chaotic gyrostat system with the aid of energies and external forces. In 2018, Chegini et al. [12] assumed two rigid panels were attached with springs in a

gyrostat to prove its chaotic nature, whereas they also investigated the existence of chaos in a satellite system [13] moving in an orbital path.

A region \mathbb{E} where iterations are defined in such a way that any initial condition in \mathbb{E} asymptotically converges to one attractor is known as a basin of attraction. Interestingly, every point in the phase space of a linear system is in the basin of attraction, whereas in nonlinear systems, points map asymptotically or directly to infinity. However, another possibility in the nonlinear case is the convergence of few initial conditions to different basins and mapping into other attractors. Mostly, researchers have considered difference equations for computing basins of attraction, such as Brett and Kulenović [14], who considered a two-species competitive model composed of difference equations with quadratic terms. In 2016, a period-two solution was taken into account for basins of attraction, where the boundaries of two basins were asymptotically stable manifolds [15] and similar work can be seen in [16]. There are also several methods provided to compute basins in discrete and fractional dynamical systems [17–19]. Since the last decade, researchers have focused on the computation of basins for chaotic systems.

Basins can also play a helpful role in finding hidden and coexisting attractors in chaotic systems [20–23]. The coexisting attractor (multistability) [24] for a set of parameters has been studied for many nonlinear systems. It identifies the nonuniqueness of the system's final state. There are concepts to deal with the complexity of a dynamical system, but the coexisting attractor is one of the recent interest. Studies have revealed that, the famous butterfly attractor in Lorenz-type systems was separated into two symmetrical attractors in [25,26], whereas Xiong et al. [27] made it possible to bring tristability in a different set of parameter. It has also been found that control methods are not only limited to help control chaos but also have a special role in finding coexisting attractors [28,29].

Synchronization is a process in which master and slave systems achieve state consistency using control inputs [30]. This topic has a variety of applications in hardware implementation for the verification of several types of attractors [31]. In 2015, Esteban et al. [32] discussed the existence of multiscrolls in chaotic systems and verified those attractors through FGPA. Moreover, synchronization plays an important role in secure communication [33,34]. In 2021, González-Zapata et al. synchronized artificial neuron chaotic systems and implemented their technique to transfer an image file in a secure way [35]. Moreover, synchronization is categorized on the basis of its properties including (complete, cluster and lag) synchronizations. All these types are further divided on the basis of identical or nonidentical synchronization [36]. In 2020, Chen [37] synchronized two identical gyrostat dynamical systems with the aid of a newly designed controller, variable substitution and a feedback controller (VSFC) to obtain global stability. Similarly, Lazaros et al. [33] used an active control strategy for the synchronization of two nonidentical systems. For two decades, researchers have been working on synchronization and utilizing it in engineering-based application [38–41]. There are some research works found on aerial vehicles in which a gyrostat was used to navigate position, but the unpredictability in a gyrostat can lead to disorder in the path navigation and losing signals with such aerial vehicles. We have noticed the following points which motivated us to continue our work.

- Qi et al. [11] modeled a gyrostat chaotic system and discussed its bifurcation using energy functions.
- In 2021, Sabir et al. [42] considered the same model of gyrostat for the existence of oscillatory solutions. The authors also worked on bringing stability to their trajectories with the help of an $M_{chaotic}$ controller.
- In 2022, Marwan et al. [43] designed a full-order generalized observer for fractional-order chaotic systems and used the same gyrostat model as an application.
- In 2015, Sprott and their team [44] provided a platform to classify and quantify basins in several planes. In 2017, Xiong et al. [27] plotted a basin of attraction in three dimensions for the first time for the Lorenz system and discussed its tristability.

From the above cited literature, we see that no one has ever discussed the basins of gyrostat systems. However, Xiong et al. [27] achieved three symmetrical basins in

the Lorenz system for a different parameter set but using the same concept we obtain multistability in a gyrostat system with infinitely many symmetrical basins. Moreover, in this work, we focus on a finding coexisting attractor in the considered system using basins of attraction. For more depth these basins are constructed in three dimensions as well, for the first time in mechanical systems, while for more novelty, the same model is synchronized with another mechanical system using an $M_{chaotic}$ controller. This controller was used for the first time by Sabir et al. [42] for controlling chaos and no one has used it for the purpose of synchronization.

This paper is organized in such a manner that in Section 2, a gyrostat chaotic system is examined to find basins of attraction in two and three dimensions, whereas several dynamical properties for a coexisting attractor are discussed in Section 3. Section 4 presents the synchronization of two nonidentical mechanical-based chaotic systems using an $M_{chaotic}$ controller, while Section 5 is the concluding part of our work.

2. Multistability of the Gyrostat System

Spacecrafts, in which rotors are fixed to a rigid body, are referred to as gyrostats. The three-dimensional autonomous system of ordinary differential equations of a gyrostat [11] is:

$$\begin{cases} I_x \dot{x} = -\mu_x x - h_z y + h_y z + (I_y - I_z) y z + L_x \\ I_y \dot{y} = h_z x + \mu_y y + (I_x - I_z) x z + L_y \\ I_z \dot{z} = -h_y x - \mu_z z + (I_x - I_y) x y + L_z. \end{cases} \tag{1}$$

In Section 4, we show the synchronized gyrostat and quadrotor chaotic systems, therefore for convenience, system (1) is simplified into:

$$\begin{cases} \dot{x}_1 = -b_{11} x_1 - b_{12} x_2 + b_{13} x_3 + F_{1m} x_2 x_3 + L_{1m} \\ \dot{x}_2 = b_{21} x_1 + b_{22} x_2 + F_{2m} x_1 x_3 + L_{2m} \\ \dot{x}_3 = -b_{31} x_1 - b_{33} x_3 + F_{3m} x_1 x_2 + L_{3m}, \end{cases} \tag{2}$$

where the changed parameters along with their values for when a system (2) is chaotic are given in Table 1; the parametric values given in Table 1 are taken from [11].

Table 1. Parametric values for Gyrostat chaotic model [11].

New Parameters	Old Parameters	Value	Units
b_{11}	$\frac{\mu_x}{I_x}$	2	$N \cdot s \cdot m^{-1} \cdot kg^{-1}$
F_{1m}	$\frac{I_y - I_z}{I_x}$	$\frac{1}{3}$	N/A
b_{12}	$\frac{h_z}{I_x}$	0.7933	s^{-1}
F_{2m}	$\frac{I_z - I_x}{I_y}$	-1	N/A
b_{13}	$\frac{h_y}{I_x}$	0.1914	s^{-1}
F_{3m}	$\frac{I_x - I_y}{I_z}$	1	N/A
b_{21}	$\frac{h_z}{I_y}$	1.19	s^{-1}
L_{1m}	$\frac{L_x}{I_x}$	0	$N \cdot m^{-1} \cdot kg^{-1}$
b_{22}	$\frac{h_z}{I_y}$	3.215	$N \cdot s \cdot m^{-1} \cdot kg^{-1}$
L_{2m}	$\frac{L_y}{I_y}$	0	$N \cdot m^{-1} \cdot kg^{-1}$
b_{31}	$\frac{h_y}{I_z}$	0.5742	s^{-1}
L_{3m}	$\frac{L_z}{I_z}$	22.8	$N \cdot m^{-1} \cdot kg^{-1}$
b_{33}	$\frac{\mu_z}{I_z}$	5.8	$N \cdot s \cdot m^{-1} \cdot kg^{-1}$

Figure 1 illustrates the chaotic trajectories of system (2) with initial conditions $(x_1, x_2, x_3) = (0.1, 0.1, 0.1)$ and parameter values given in Table 1. An interesting property of Equation (2) is that for some values of the bifurcation parameter, the system shows more

than one stable chaotic attractor. So, in this section we investigated the basin, which is the set of points that asymptotically approaches a certain attractor as time advances.

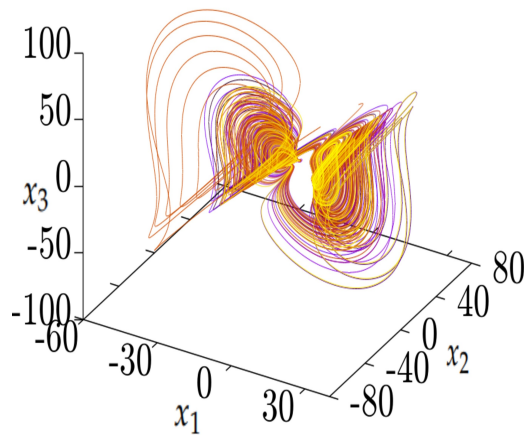


Figure 1. Chaotic attractor of system (2).

For a decade, researchers have been working on the computation of basins by cross-sectioning, and Figure 2 is the same plot of the gyrostat system with a slightly changed parameter value of b_{22} .

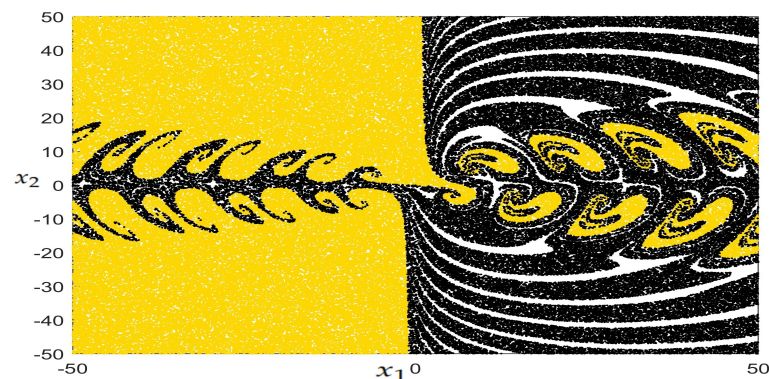


Figure 2. Two-dimensional cross-section of basin of attraction at $x_3 = 0$ for $b_{22} = 3.9$ based on discrete points with the aid of MATLAB.

It can be observed from Figure 1 and the cross-section of the basin at $x_3 = 0$ that the gyrostat had a global attractor before changing its parameter value, b_{22} , but the 2D cross-section of the basins of attraction at $x_3 = 0$ indicates the complexity of the basins, consisting of discrete points connected through three colors (yellow, black and white). These colors are categorized as points consisting of yellow for the first basin, black colored points for the second basin, whereas white colored points in Figure 2 approach infinity. Figure 2 also shows the existence of infinitely many symmetrical fractals by breaking the chaotic attractor of system (2), but for simplicity, we have limited the range of our findings to the interval $J = [-50, 50]$.

In systems of multiple attractors, it is possible to observe more than one basin and sometimes the structure of boundaries between the basins might be very complex. Such complexities may lead to a phenomenon called final state sensitivity, in which the boundary shows a fractal pattern [18,27].

For the bifurcation parameter $b_{22} = 3.48$ the system shows three stable chaotic attractors. In Figure 3a we plotted the intersection of the basins with the planes $x_{10} = 0$, $x_{20} = 0$ and $x_{30} = 0$. The initial conditions in each region converge to the attractor plotted with the same color as in Figure 3b.

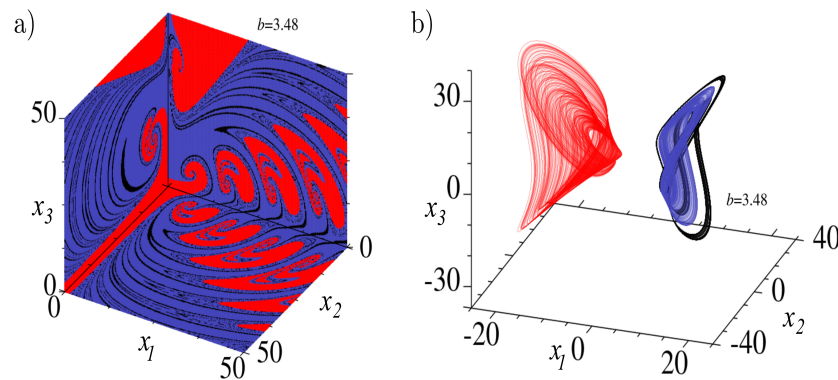


Figure 3. (a) Intersections of the basins of attraction of Equation (2) with the planes $x_{10} = 0$, $x_{20} = 0$ and $x_{30} = 0$. For the parameter value $b_{22} = 3.48$, the system presents three stable chaotic attractors, depicted in (b).

We studied the basin of attraction in the considered system for multistability. Dynamical systems with multiple attractors obey the property that each basin of attraction divides the space into separated regions where points eventually approach each attractor.

As shown in Figures 4 and 5, different basins are indicated using various colors. In Figure 5 a three-dimensional version of the basins are observed. The figures were generated using a grid of $120 \times 120 \times 120$ and recording the final state of each initial condition after some transient time. The boundary between the basins of the red and the blue attractors can be seen as smooth and well-defined. However, basins of the blue and black attractors are intermingled, which increases the final state sensitivity and impacts the predictability of the dynamical behavior. Another information we can take from Figures 3 and 4 is that although the red attractor may be characterized by $x < 0$, it is possible for a dynamical orbit to approach this attractor even if its initial condition is given by $x_1 > 0$, by adjusting the values of x_{20} and x_{30} . This is also true for the blue and black attractors, although more care must be taken in this case due to the complexity of the boundary.

In Figure 5a, the points in the first basin with the red color are of the attractor centered at $(-10.5, -1.37, 2.08)$, and the yellow points observed in Figure 5b are in the second basin of the attractor centered at $(9.5, -1.37, 2.08)$. According to the classification in [44], these basins fall into the “type 1” category.

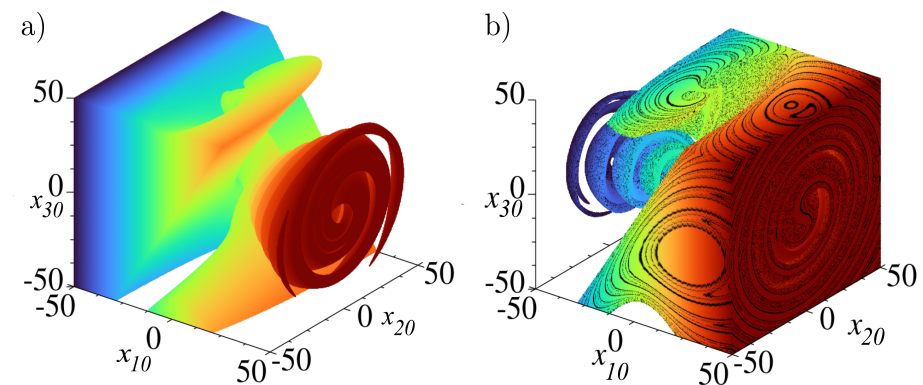


Figure 4. Three-dimensional basin of attraction on a grid of $120 \times 120 \times 120$ points. In (a), we plotted the basin of attraction of the red attractor of Figure 3b. In (b), the colored region is the basin of the blue attractor of Figure 3b, while the black region is the basin of the black attractor.

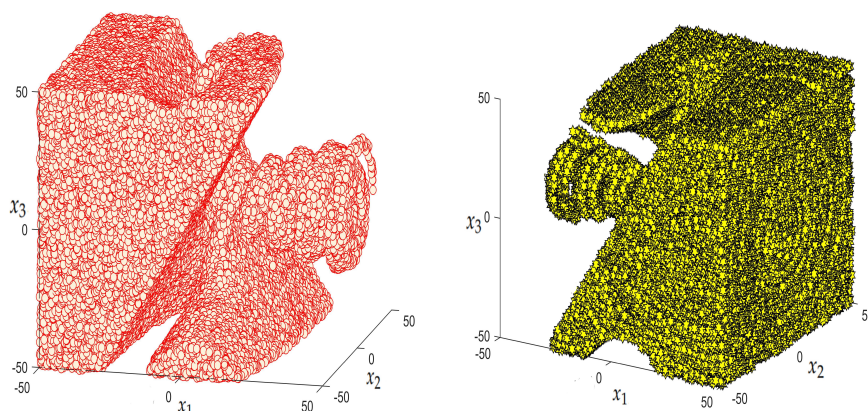


Figure 5. Three-dimensional basin of attraction based on 10 million discrete points using MATLAB.

Most previous studies on basins are focused on cross-sections in $2D$, while there is also a $3D$ example of a basin plot such as in [27] for the tristability of the Lorenz system, but we obtained results for multistability using FORTRAN and MATLAB in continuous and discrete points, which can be seen in Figures 4 and 5, respectively. Both results in Figures 4 and 5 look similar; the difference is that the results achieved using FORTRAN with eight processors are informative and good-looking from a reader's end. However, the results obtained with the aid of MATLAB were using four processors and were represented in a discrete way, which can provide more information for the readers by zooming on it.

Studying the basins of attraction gives us information on the system, such as the region of stability, which is crucial in certain problems including our system. By studying the region of basins, we were able to predict the future behavior of points in the space, such as whether they would escape to infinity or be attracted to an attractor. Different states of the gyrostat, such as being chaotic or not, affect the use of it in spacecrafts and a comprehensive knowledge will give astronauts better control to it.

3. Coexisting Attractor Extracted from Second Basin

In Section 2, we saw that some trajectories were approaching towards another region and stayed there, which indicated the existence of another attractor in the system (2). In this section, the analysis of system (2) was performed using famous tools such as a bifurcation diagrams, Lyapunov exponents and the Poincaré section, using the Runge–Kutta algorithm. Moreover, for each simulation in this paper, the time step was $\Delta t = 0.001$. In Figure 6, the bifurcation diagrams of coexisting (red color) and chaotic attractors (blue) were plotted for a damping coefficient b_{22} in the range $[0, 4]$. In order to perform a deeper analysis of the bifurcations, we divided Figure 6 into six subregions, R_1 – R_6 , and each region is enclosed in various colored rectangles.

As the damping coefficient starts from zero, two single lines in red and blue colors emerge for $b_{22} \in [0, 1.25]$ as illustrated in Figure 7a, which shows the nonexistence of the bifurcation, but as the damping coefficient crosses $b_{22} = 1.25$, the bifurcation starts to take place in R_2 , which is more visible in Figure 7b for $b_{22} \in (1.25, 1.5)$.

Jumping into regions R_3 – R_5 shown in Figure 7c–e, a number of bifurcations are observed with uncountable periodicity and eddy-type trajectories in which nothing can be predicted about the trajectories except chaos. Here, it is interesting to discuss that a chaotic region lies in the middle, because as we increase the value of the damping coefficient b_{22} towards 4, again, a predictable period of bifurcation can be seen in Figure 7f, which ends with the property that the period 6 bifurcation shrinks into a period-doubling bifurcation for both attractors.

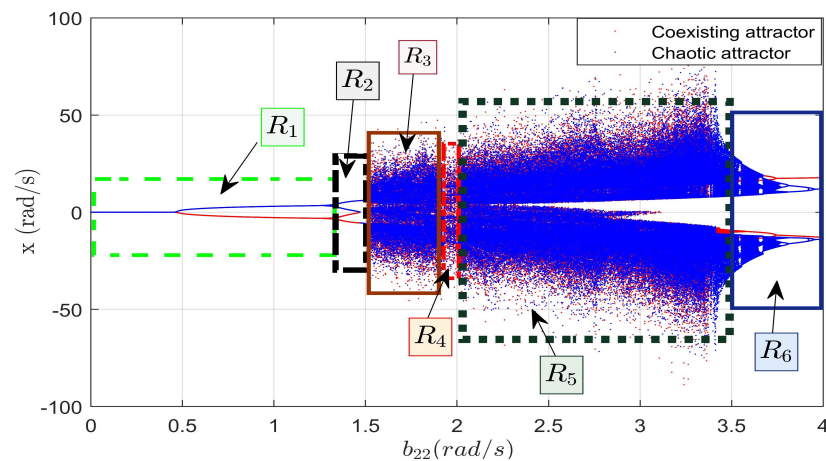


Figure 6. Bifurcation diagram in the second basin for the coexisting attractor in system (2).

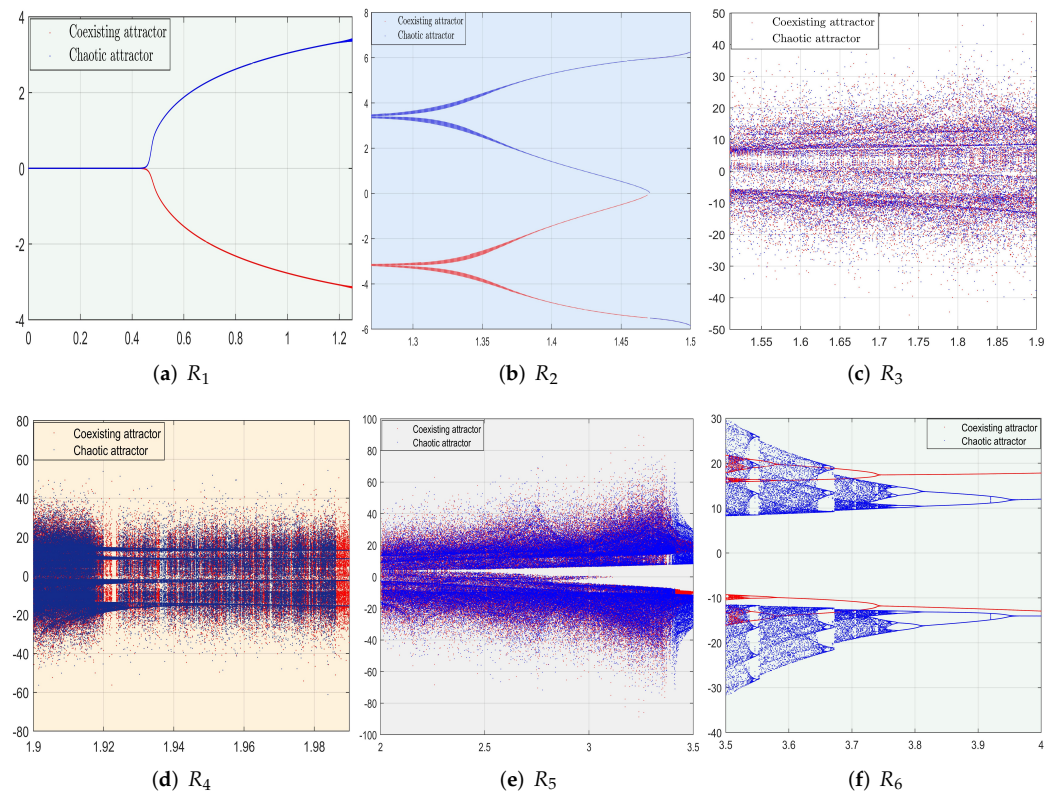


Figure 7. Bifurcation diagram partitioned in subregions (bifurcation leading to chaos).

Chaos in dynamical systems depends on many factors, but the sensitivity to initial conditions is one of the main factors. Therefore, perturbing the initial conditions in chaotic systems can verify its chaotic nature, and may lead to the concept of Lyapunov exponents. After perturbation, if the system has a stable solution, then nearby trajectories will come closer exponentially, while in the chaotic case, with a negligible perturbation nearby trajectories will separate exponentially.

In Figure 8, the Lyapunov exponents diagram with respect to the bifurcation parameter b_{22} were plotted. The exponents were calculated according to the algorithm proposed by Wolf [45] considering the same initial condition for each value of b_{22} , so although it was useful to investigate the presence of chaos, this diagram was not able to indicate the presence of effects such as bi- or tristability.

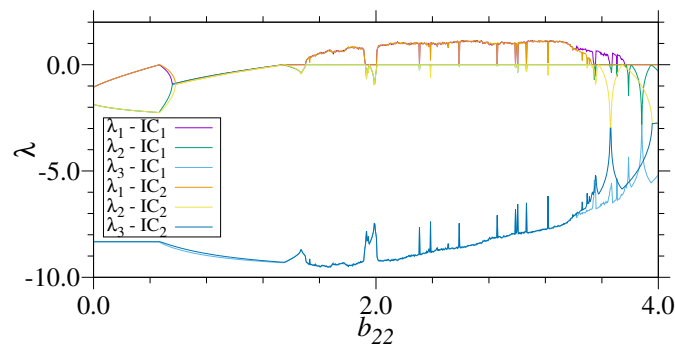


Figure 8. Lyapunov exponents λ_i for $i = 1, 2, 3$ at each value of bifurcation parameter b_{22} .

From Figure 8, it is observed that the dynamics in system (1) for both (strange and coexisting) attractors exhibit unpredictability at $b_{22} \approx 1.5$, when the first Lyapunov exponent becomes greater than zero. The dynamics remains mostly chaotic till $b_{22} \approx 3.78$ and then converges towards a limit cycle again. Inside the range of b_{22} , we can also observe the presence of periodic windows, which are associated with the shrimp-shaped structures observed in the parameter space.

Lyapunov exponents can be achieved for each value of the bifurcation parameter as shown in Figure 8, but one can also verify the Lyapunov exponents for single values. In Figure 9, there are six Lyapunov exponents where $(\lambda_{1,1}, \lambda_{1,2}, \lambda_{1,3}) = (0.7, 0, -5.34)$ represent the chaotic attractor belonging to the first basin, whereas $(\lambda_{2,1}, \lambda_{2,2}, \lambda_{2,3}) = (0.6, 0, -5.32)$ represent the coexisting attractor belonging to the second basin. Chlouverakis and Sprot in 2005 modified the Kaplan–Yorke dimension D_{XY} [46] and reported that D_{XY} belonged to interval $I = [2, 3]$ for any dynamical system showing the existence of chaos. Hence, in both our cases,

$$D_{XY} = 1.5 + 0.5\sqrt{1 - \frac{8\lambda_a}{\lambda_c}} \tag{3}$$

We obtained $D_{1XY} = 2.215662$ and $D_{2XY} = 2.189611$ for the chaotic and coexisting attractors, respectively, using Equation (3). As D_{1XY} and D_{2XY} both belonged to interval $I = [2, 3]$, therefore, the coexisting attractor was confirmed in system (2).

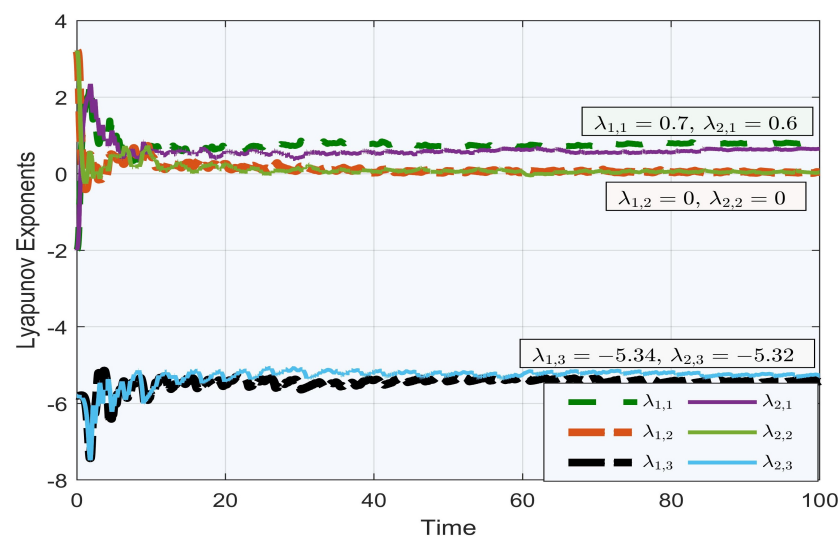


Figure 9. Lyapunov exponents $\lambda_{1,i}; i = 1, 2, 3$ for the chaotic attractor and $\lambda_{2,i}; i = 1, 2, 3$ for the coexisting attractor.

A further study in dynamical analysis reveals that the Poincaré section is also one of the tools which plays a fundamental role in detecting chaos. Apart from getting information

about chaos, one can also obtain whether the obtained solution is periodic or not. It is worth noting that Poincaré sections have recently been used to detect chaotic behavior in fractional order systems with hidden attractors [47]. Moreover, it is also important to mention that the dimension of a Poincaré section (PS) is always one less than the dimension of its corresponding dynamical system (DS):

$$\dim(\text{PS}) = \dim(\text{DS}) - 1. \tag{4}$$

The reason behind the dimension in Equation (4) is the intersection of the orbits generated from the solution of the dynamical system with the plane in each direction.

For convenience, we have plotted the coexisting attractor along with the chaotic attractor. In Figure 10, two subfigures in the x_1 - x_2 plane can be observed, in which Figure 10a illustrates the Poincaré section of both attractors and indicates an unlimited number of points after passing through the x_1 - x_2 plane. All these points illustrate the existence of chaos, whereas Figure 10b shows the phase portraits of both attractors. Moreover, the attractor given in blue color belongs to the first basin, while the attractor with red color is in the second basin.

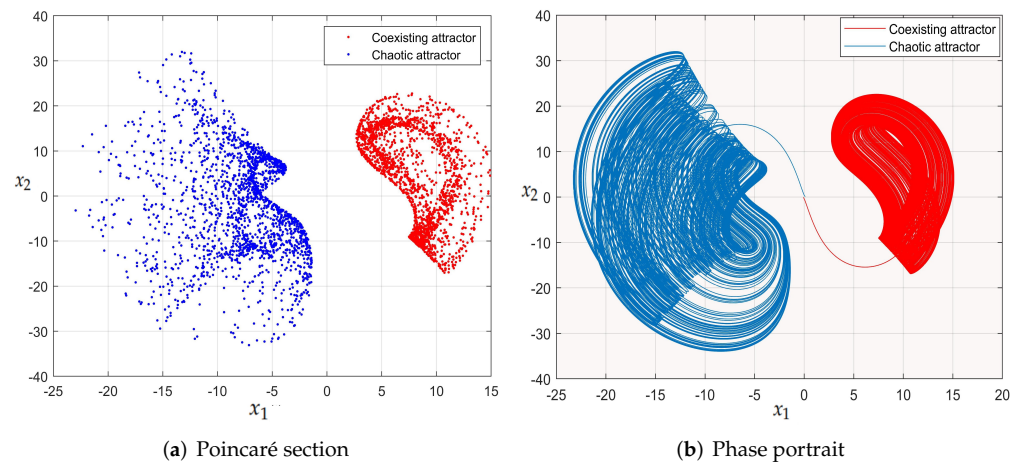


Figure 10. Poincaré section and corresponding phase portrait of chaotic attractor vs. coexisting attractor in system (2) for $x_1 - x_2$ plane.

The explanation for other two planes, x_2 - x_3 and x_1 - x_3 is similar and shown in Figures 11 and 12, respectively.

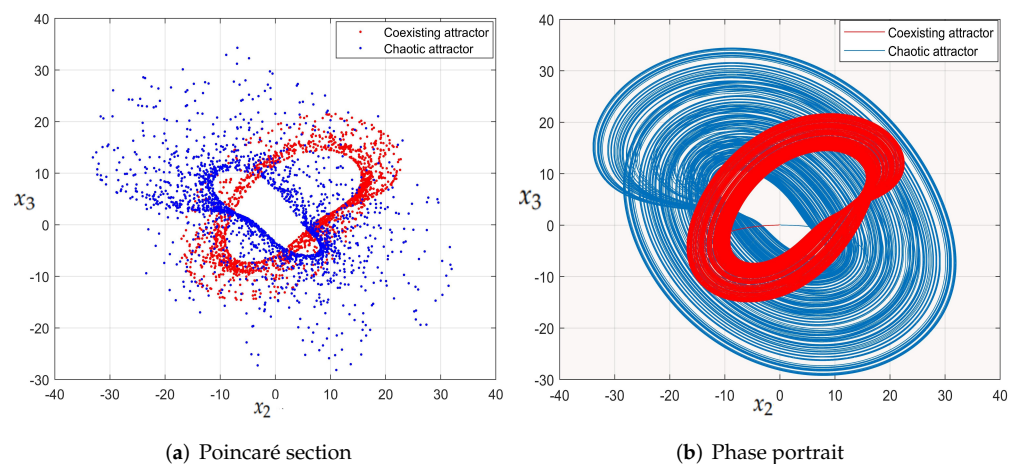


Figure 11. Poincaré section and corresponding phase portrait of chaotic attractor vs. coexisting attractor in system (2) for $x_2 - x_3$ plane.

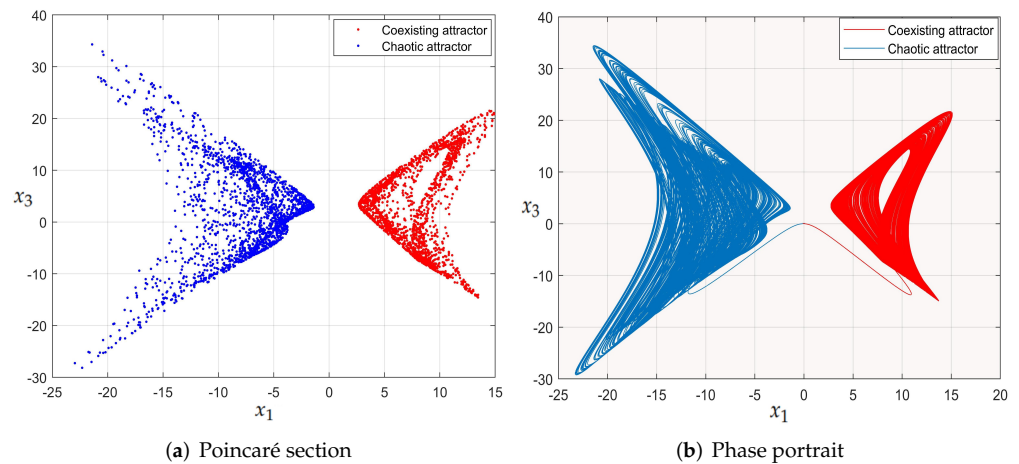


Figure 12. Poincaré section and corresponding phase portrait of chaotic attractor vs. coexisting attractor in system (2) for x_1 - x_3 plane.

4. Synchronization of Two Nonidentical Mechanical Systems Using $M_{chaotic}$ Controller

Synchronization is a famous procedure used for adapting the properties of a master system. This phenomenon became well-known after the publications of [48–50], where the author used a control input for overlapping trajectories of a slave system over a master system. In other words, we can say that after some time “ t ”, the slave system will start following the trajectories of the master system.

Definition 1 ([51]). *Let us suppose $V : x \rightarrow V(x)$ is a Lyapunov function, then $V(x)$ is negative definite if it satisfies the following properties:*

$$V(x) > 0, \quad \forall x, \tag{5}$$

$$\frac{dV}{dx} \leq 0, \quad \forall x. \tag{6}$$

In 2021, Sabir et al. [42] designed an $M_{chaotic}$ controller for controlling chaos, therefore, in this section, we used (Algorithm 1, [42]) for the synchronization of two mechanical systems. For this, the master system was considered to be a gyrostat chaotic system (2) and a quadrotor unmanned aerial vehicle (QUAV) system (8) was taken as the slave system.

Theorem 1. *The trajectories of a QUAV chaotic system (8) are synchronized with gyrostat system (2) using $M_{chaotic}$ controller $M_i = A_i + W_i, i = 1, 2, 3$, where $A_i = Sx + N(e, x) + k$ with,*

$$S = \begin{pmatrix} a_{11} - b_{11} & a_{12} - b_{12} & b_{13} \\ -a_{21} + b_{21} & a_{22} + b_{22} & 0 \\ -b_{31} & 0 & a_{33} - b_{33} \end{pmatrix}, N(e, x) = \begin{pmatrix} -F_{1s}(e_2e_3 + x_2e_3 + e_2x_3) \\ -F_{2s}(e_1e_3 + x_1e_3 + e_1x_3) \\ -F_{3s}(e_1e_2 + x_1e_2 + e_1x_2) \end{pmatrix}, \tag{7}$$

$$k = \begin{pmatrix} (F_{1m} - F_{1s})x_2x_3 + L_{1m} \\ (F_{2m} - F_{2s})x_1x_3 + L_{2m} \\ (F_{3m} - F_{3s})x_1x_2 + L_{3m} \end{pmatrix}, W_i = \begin{pmatrix} (\bar{a}_{11} - \rho) & \bar{a}_{12} & 0 \\ -\bar{a}_{21} & (\bar{a}_{22} - \rho) & 0 \\ 0 & 0 & (\bar{a}_{33} - \rho) \end{pmatrix} \begin{pmatrix} e_1 \\ e_2 \\ e_3 \end{pmatrix}.$$

Proof. We start the proof of Theorem 1 by following the steps of the algorithm given in [42]. In step 1, we add time-dependent control inputs $M_i(t)$ to each equation of the slave system:

$$\begin{cases} \dot{y}_1 = -a_{11}y_1 - a_{12}y_2 + F_{1s}y_2y_3 + M_1(t) \\ \dot{y}_2 = a_{21}y_1 - a_{22}y_2 + F_{2s}y_1y_3 + M_2(t) \\ \dot{y}_3 = -a_{33}y_3 + F_{3s}y_1y_2 + \Omega + M_3(t). \end{cases} \tag{8}$$

Then, the error terms, the difference between the state variables of system (2) and (8)

$$\begin{cases} e_1 = y_1 - x_1, \\ e_2 = y_2 - x_2, \\ e_3 = y_3 - x_3, \end{cases} \tag{9}$$

can be used to obtain the error dynamical system by differentiating Equation (9)

$$\begin{aligned} \dot{e}_1 &= -a_{11}e_1 - a_{11}x_1 - a_{12}e_2 - a_{12}x_2 + b_{11}x_1 + b_{12}x_2 - b_{13}x_3 \\ &\quad + F_{1s}y_2y_3 - F_{1m}x_2x_3 - L_{1m} + M_1(t), \\ \dot{e}_2 &= a_{21}e_1 + a_{21}x_1 - a_{22}e_2 - a_{22}x_2 - b_{21}x_1 - b_{22}x_2 + F_{2s}y_1y_3 \\ &\quad - F_{2m}x_1x_3 - L_{2m} + M_2(t), \\ \dot{e}_3 &= -a_{33}e_3 - a_{33}x_3 + b_{31}x_1 + b_{33}x_3 + F_{3s}y_1y_2 - F_{3m}x_1x_2 \\ &\quad - L_{3m} + \Omega + M_3(t). \end{aligned} \tag{10}$$

$M_i(t)$ is further composed of two parts. First, we find A_i , $i = 1, 2, 3$, using an active control strategy:

$$\begin{aligned} \begin{pmatrix} A_1 \\ A_2 \\ A_3 \end{pmatrix} &= \begin{pmatrix} (a_{11} - b_{11})x_1 + (a_{12} - b_{12})x_2 + b_{13}x_3 \\ (b_{21} - a_{21})x_1 + (a_{22} + b_{22})x_2 \\ -b_{31}x_1 + (a_{33} - b_{33})x_3 \end{pmatrix} + \\ &\begin{pmatrix} -F_{1s}(e_2e_3 + x_2e_3 + e_2x_3) + (F_{1m} - F_{1s})x_2x_3 + L_{1m} + W_1 \\ -F_{2s}(e_1e_3 + x_1e_3 + e_1x_3) + (F_{2m} - F_{2s})x_1x_3 + L_{2m} + W_2 \\ -F_{3s}(e_1e_2 + x_1e_2 + e_1x_2) + (F_{3m} - F_{3s})x_1x_2 + L_{3m} - \Omega + W_3 \end{pmatrix}. \end{aligned} \tag{11}$$

The error dynamical system can be simplified by putting Equation (11) into Equation (10):

$$\begin{aligned} \dot{e}_1 &= -a_{11}e_1 - a_{12}e_2 + W_1, \\ \dot{e}_2 &= a_{21}e_1 - a_{22}e_2 + W_2, \\ \dot{e}_3 &= -a_{33}e_3 + W_3. \end{aligned} \tag{12}$$

However, the second part W_i of controller M_i is still there. To find W_i , we assume that the remaining parameters are anonymous and the limiting value of the solution of Equation (12) approaches zero as time advances

$$\begin{aligned} W_1 &= -k_1e_1 + (\bar{a}_{11} - \rho)e_1 + \bar{a}_{12}e_2, \\ W_2 &= -k_2e_2 + \bar{a}_{21}e_1 + (\bar{a}_{22} - \rho)e_2, \\ W_3 &= -k_3e_3 + (\bar{a}_{33} - \rho)e_3, \end{aligned} \tag{13}$$

where $k_i > 0$, $i = 1, 2, 3$, are gain values, ρ is the desired eigenvalue and \bar{a}_{11} , \bar{a}_{12} , \bar{a}_{21} , \bar{a}_{22} , \bar{a}_{33} are estimated parameters of a_{11} , a_{12} , a_{21} , a_{22} , a_{33} , respectively. Substituting back Equation (13) into Equation (12) yields:

$$\begin{aligned} \dot{e}_1 &= -(k_1 + \rho)e_1 - \Gamma_{11}e_1 - \Gamma_{12}e_2, \\ \dot{e}_2 &= -(k_2 + \rho)e_2 + \Gamma_{21}e_1 - \Gamma_{22}e_2, \\ \dot{e}_3 &= -(k_3 + \rho)e_3 - \Gamma_{33}e_3, \end{aligned} \tag{14}$$

where $\Gamma_k = a_k - \bar{a}_k(t)$ for $k = (11), (12), (21), (22), (33)$. In the final step, we need to find anonymous time-dependent parameters using a quadratic Lyapunov function:

$$T(e) = \frac{1}{2} \left(e_1^2 + e_2^2 + e_3^2 + \Gamma_{11}^2 + \Gamma_{12}^2 + \Gamma_{21}^2 + \Gamma_{22}^2 + \Gamma_{33}^2 \right). \tag{15}$$

Moreover, Equation (15) satisfies the first condition of Definition 1, because $T(e)$ is quadratic and will be positive for all values of e . However, to achieve the second condition of Definition 1, we need to differentiate $T(e)$ with respect to their corresponding trajectories and use Equation (14) into the differentiation of Equation (15):

$$\begin{aligned} \frac{dT(e)}{dt} = & -(k_1 + \rho)e_1^2 - (k_2 + \rho)e_2^2 - (k_3 + \rho)e_3^2 + \Gamma_{11}(\dot{\Gamma}_{11} - e_1^2) + \Gamma_{12} \times \\ & (\dot{\Gamma}_{12} - e_1e_2) + \Gamma_{21}(\dot{\Gamma}_{21} + e_1e_2) + \Gamma_{22}(\dot{\Gamma}_{22} - e_2^2) + \Gamma_{33}(\dot{\Gamma}_{33} - e_3^2). \end{aligned} \tag{16}$$

The following updated parameter law (17) can be used for achieving $\frac{dT(e)}{dt}$ to be negative definite:

$$\begin{cases} \dot{\Gamma}_{11} = -k_4\Gamma_{11} + e_1^2 \\ \dot{\Gamma}_{12} = -k_5\Gamma_{12} + e_1e_2 \\ \dot{\Gamma}_{21} = -k_6\Gamma_{21} - e_1e_2 \\ \dot{\Gamma}_{22} = -k_7\Gamma_{22} + e_2^2 \\ \dot{\Gamma}_{33} = -k_8\Gamma_{33} + e_3^2. \end{cases} \tag{17}$$

Using Equation (17) into Equation (16) yields:

$$\frac{dT(e)}{dt} = -\Lambda, \tag{18}$$

where $\Lambda = (k_1 + \rho)e_1^2 + (k_2 + \rho)e_2^2 + (k_3 + \rho)e_3^2 + k_4\Gamma_{11}^2 + k_5\Gamma_{12}^2 + k_6\Gamma_{21}^2 + k_7\Gamma_{22}^2 + k_8\Gamma_{33}^2$. Solving Equation (18) by the variable separable method yields:

$$T(e) = \exp(-\Lambda t). \tag{19}$$

Hence, we get our desired result from Equation (19) that, as t tends to infinity, $T(e)$ approaches zero. This shows that, the considered Lyapunov function is dissipative and $y(t)$ will start following $x(t)$ when the error term approaches zero. \square

Graphical Validation of Theorem 1

Mathematically, the results given in Theorem 1 with the $M_{chaotic}$ controller ensure that the trajectory of the QUAV system synchronizes with the gyrostat chaotic system. However, numerical simulations were conducted to validate the analytical work given in Equations (11)–(19).

Figure 13 is a phase portrait of system (8) following the path of system (2) in which trajectories are observed in three different colors. The trajectory in yellow color represents Equation (2) and is considered as the master system. The green colored trajectory shows the slave system and the blue color illustrates the error between master and slave systems. As the estimated parameters start approaching their original values, using the parameter updated law (17), the error terms $e_i = y_i - x_i, i = 1, 2, 3$, tend to zero which indicate the slave system in green color will converge towards the master system as time advances.

Figure 14 shows the time history of Figure 13, which illustrates that the trajectories of system (8) emerge from their initial points and overlap x_1, x_2 and x_3 with the advancement in time. For convenience, an area where synchronization occurs is visualized in more depth in zoomed-in inserts. Here, the dotted lines are for y_1, y_2 and y_3 and the full lines shows x_1, x_2 and x_3 . In each zoomed-in insert, the dotted lines join the full lines at a specific point and follow these lines till the end, which confirms the occurrence of synchronization.

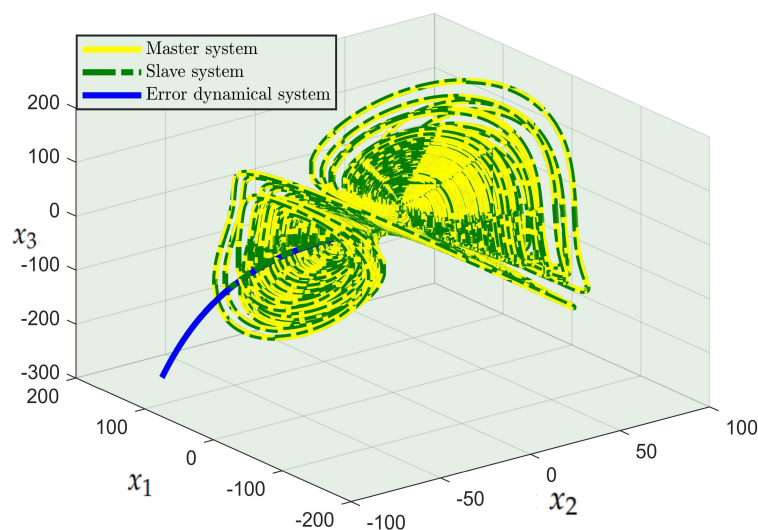


Figure 13. Synchronization of master and slave systems.

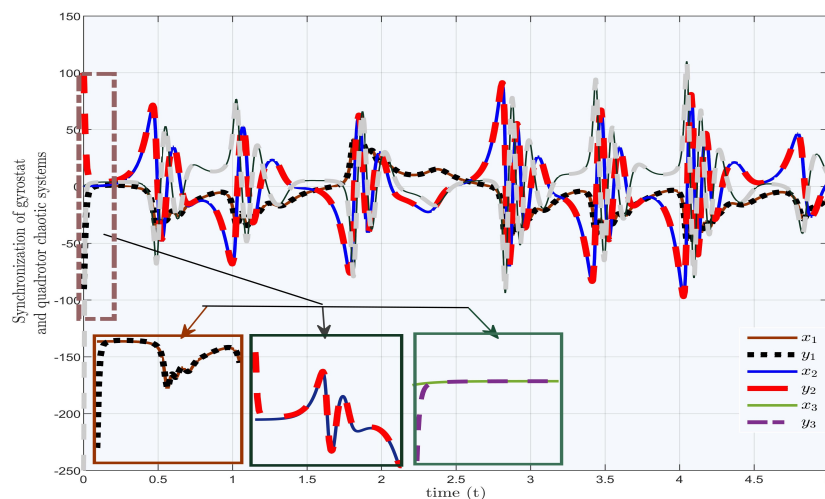


Figure 14. Time history of master and slave systems

5. Conclusions

In this research, for the first time, a coexisting attractor in the gyrostat system was examined utilizing basins of attraction, and the technique for searching basins employed in the current work was also reliable for computers with two or four processors. Furthermore, the same approach was used in the current study to shatter the chaotic attractor of the considered model into an endless number of fractals, as seen in Figure 2. For the first time in a spacecraft model, a three-dimensional basin of attraction was plotted to determine the existence of a coexisting attractor in the considered model. For the confirmation and illustration of the coexisting attractor, certain basic dynamical features were applied. Moreover, a newly built controller was employed in the second portion of this study for synchronizing two mechanical systems. This concept was explained in more detail with the help of Figure 14, in which the trajectories of a QUAV system started approaching the trajectories of our considered model and followed their pattern till the end.

Author Contributions: Conceptualization, M.M., V.D.S. and A.X.; methodology, M.M. and V.D.S.; software, M.M., V.D.S., M.Z.A. and A.X.; validation, M.M., V.D.S., M.Z.A. and A.X.; formal analysis, M.M. and V.D.S.; investigation, M.M. and M.Z.A.; resources, M.M.; writing—original draft preparation, M.M., V.D.S. and A.X.; writing—review and editing, M.M., V.D.S., M.Z.A. and A.X.; supervision, M.M.; project administration, M.M. and M.Z.A. All authors have read and agreed to the published version of the manuscript.

Funding: This research received no external funding.

Institutional Review Board Statement: Not Applicable.

Informed Consent Statement: This paper does not contain any studies with human participants or animals performed by any of the author.

Data Availability Statement: MATLAB and FORTRAN codes are available upon reasonable request from the corresponding author.

Conflicts of Interest: All authors declare no conflict of interest.

References

1. Vaios, L. A Control Moment Gyro (CMG) Based Attitude Control System (ACS) for Agile Small Satellites. Ph.D. Thesis, University of Surrey, Guildford, UK, 2002.
2. Jalili, M.M.; Emami, H. Analytical solution for nonlinear oscillation of workpiece in turning process. *Proc. Inst. Mech. Eng. Part C J. Mech. Eng. Sci.* **2017**, *231*, 3479–3492. [[CrossRef](#)]
3. Pivarčiová, E.; Božek, P.; Turygin, Y.; Zajačko, I.; Shchenyatsky, A.; Václav, Š.; Císar, M.; Gemela, B. Analysis of control and correction options of mobile robot trajectory by an inertial navigation system. *Int. J. Adv. Robot. Syst.* **2018**, *15*, 1729881418755165. [[CrossRef](#)]
4. Qazizada, M.E.; Pivarčiová, E. Mobile robot controlling possibilities of inertial navigation system. *Procedia Eng.* **2016**, *149*, 404–413. [[CrossRef](#)]
5. Kose, E.; Muhurcu, A. Comparative Controlling of the Lorenz Chaotic System Using the SMC and APP Methods. *Math. Probl. Eng.* **2018**, *2018*, 9612749. [[CrossRef](#)]
6. Lu, X. A Financial Chaotic System Control Method Based on Intermittent Controller. *Math. Probl. Eng.* **2020**, *2020*, 5810707. [[CrossRef](#)]
7. Iqbal, J.; Ahmad, S.; Marwan, M.; Shaukat, M. Archive of Applied Mechanics. *Cont. Numer. Anal. Cancer Chaotic Syst.* **2020**, *90*, 2597–2608.
8. Aslanov, V.; Yudintsev, V. Dynamics and chaos control of gyrostat satellite. *Chaos Solitons Fractals* **2012**, *45*, 1100–1107. [[CrossRef](#)]
9. Kuang, J.; Tan, S.; Arichandran, K.; Leung, A. Chaotic attitude motion of gyrostat satellite via Melnikov method. *Int. J. Bifurc. Chaos* **2001**, *11*, 1233–1260. [[CrossRef](#)]
10. Abtahi, S.M. Melnikov-based analysis for chaotic dynamics of spin-orbit motion of a gyrostat satellite. *Proc. Inst. Mech. Eng. Part K J. Multi-Body Dyn.* **2019**, *233*, 931–941. [[CrossRef](#)]
11. Qi, G.; Yang, X. Modeling of a chaotic gyrostat system and mechanism analysis of dynamics using force and energy. *Complexity* **2019**, *2019*, 5439596. [[CrossRef](#)]
12. Chegini, M.; Sadati, H.; Salarieh, H. Chaos analysis in attitude dynamics of a flexible satellite. *Nonlinear Dyn.* **2018**, *93*, 1421–1438. [[CrossRef](#)]
13. Chegini, M.; Sadati, H.; Salarieh, H. Analytical and numerical study of chaos in spatial attitude dynamics of a satellite in an elliptic orbit. *Proc. Inst. Mech. Eng. Part C J. Mech. Eng. Sci.* **2019**, *233*, 561–577. [[CrossRef](#)]
14. Brett, A.; Kulenović, M.R. Basins of attraction for two-species competitive model with quadratic terms and the singular Allee effect. *Discret. Dyn. Nat. Soc.* **2015**, *2015*, 847360. [[CrossRef](#)]
15. Bilgin, A.; Kulenović, M.R.; Pilav, E. Basins of attraction of period-two solutions of monotone difference equations. *Adv. Differ. Equ.* **2016**, *2016*, 74. [[CrossRef](#)]
16. Garić-Demirović, M.; Kulenović, M.; Nurkanović, M. Basins of attraction of equilibrium points of second order difference equations. *Appl. Math. Lett.* **2012**, *25*, 2110–2115. [[CrossRef](#)]
17. Taborda, J.A.; Angulo, F. Computing and controlling basins of attraction in multistability scenarios. *Math. Probl. Eng.* **2015**, *2015*, 313154. [[CrossRef](#)]
18. Okamoto, K.; Aoi, S.; Obayashi, I.; Kokubu, H.; Senda, K.; Tsuchiya, K. Fractal mechanism of basin of attraction in passive dynamic walking. *Bioinspiration Biomim.* **2020**, *15*, 55002. [[CrossRef](#)]
19. Liu, L.; Tian, Y.; Huang, X. A method to estimate the basin of attraction of the system with impulse effects: Application to the biped robots. In Proceedings of the International Conference on Intelligent Robotics and Applications, Wuhan, China, 15–17 October 2008; Springer: Berlin/Heidelberg, Germany, 2008; pp. 953–962.
20. Dong, C. Dynamics, Periodic Orbit Analysis, and Circuit Implementation of a New Chaotic System with Hidden Attractor. *Fractal Fract.* **2022**, *6*, 190. [[CrossRef](#)]
21. Ding, L.; Cui, L.; Yu, F.; Jin, J. Basin of Attraction Analysis of New Memristor-Based Fractional-Order Chaotic System. *Complexity* **2021**, *2021*, 5578339. [[CrossRef](#)]
22. Luo, W.; Ou, Q.; Yu, F.; Cui, L.; Jin, J. Analysis of a new hidden attractor coupled chaotic system and application of its weak signal detection. *Math. Probl. Eng.* **2020**, *2020*, 8849283. [[CrossRef](#)]
23. Zhang, X. Constructing a chaotic system with any number of attractors. *Int. J. Bifurc. Chaos* **2017**, *27*, 1750118. [[CrossRef](#)]
24. Zhu, Y.; Shang, H. Multistability of the Vibrating System of a Micro Resonator. *Fractal Fract.* **2022**, *6*, 141. [[CrossRef](#)]
25. Li, C.; Sprott, J.C.L. Multistability in a butterfly flow. *Int. J. Bifurc. Chaos* **2013**, *23*, 1350199. [[CrossRef](#)]

26. Li, C.; Sprott, J.C.L. Coexisting hidden attractors in a 4-D simplified Lorenz system. *Int. J. Bifurc. Chaos* **2014**, *24*, 1450034. [[CrossRef](#)]
27. Xiong, A.; Sprott, J.C.; Lyu, J.; Wang, X. 3D printing—The basins of tristability in the Lorenz system. *Int. J. Bifurc. Chaos* **2017**, *27*, 1750128. [[CrossRef](#)]
28. Lai, Q.; Chen, S. Generating multiple chaotic attractors from Sprott B system. *Int. J. Bifurc. Chaos* **2016**, *26*, 1650177. [[CrossRef](#)]
29. Li, C.; Thio, W.; Sprott, J.; Iu, H.; Xu, Y. Constructing infinitely many attractors in a programmable chaotic circuit. *IEEE Access* **2018**, *6*, 29003–29012. [[CrossRef](#)]
30. He, Y.; Zheng, S.; Yuan, L. Dynamics of Fractional-Order Digital Manufacturing Supply Chain System and Its Control and Synchronization. *Fractal Fract.* **2021**, *5*, 128. [[CrossRef](#)]
31. Guillén-Fernández, O.; Meléndez-Cano, A.; Tlelo-Cuautle, E.; Núñez-Pérez, J.C.; Rangel-Magdaleno, J.D.J. On the synchronization techniques of chaotic oscillators and their FPGA-based implementation for secure image transmission. *PLoS ONE* **2019**, *14*, e0209618. [[CrossRef](#)] [[PubMed](#)]
32. Tlelo-Cuautle, E.; Rangel-Magdaleno, J.; Pano-Azucena, A.D.; Obeso-Rodelo, P.; Nuñez-Perez, J.C. FPGA realization of multi-scroll chaotic oscillators. *Commun. Nonlinear Sci. Numer. Simul.* **2015**, *27*, 66–80. [[CrossRef](#)]
33. Moysis, L.; Gupta, M.K.; Mishra, V.; Marwan, M.; Volos, C. Observer design for rectangular descriptor systems with incremental quadratic constraints and nonlinear outputs—Application to secure communications. *Int. J. Robust Nonlinear Control* **2020**, *30*, 8139–8158. [[CrossRef](#)]
34. Sabir, M.; Marwan, M.; Ahmad, S.; Fiaz, M.; Khan, F. Observer and descriptor satisfying incremental quadratic constraint for class of chaotic systems and its applications in a quadrotor chaotic system. *Chaos Solitons Fractals* **2020**, *137*, 109874. [[CrossRef](#)] [[PubMed](#)]
35. González-Zapata, A.M.; Tlelo-Cuautle, E.; Cruz-Vega, I.; León-Salas, W.D. Synchronization of chaotic artificial neurons and its application to secure image transmission under MQTT for IoT protocol. *Nonlinear Dyn.* **2021**, *104*, 4581–4600. [[CrossRef](#)]
36. López-Mancilla, D.; López-Cahuich, G.; Posadas-Castillo, C.; Castañeda, C.; García-López, J.; Vázquez-Gutiérrez, J.; Tlelo-Cuautle, E. Synchronization of complex networks of identical and nonidentical chaotic systems via model-matching control. *PLoS ONE* **2019**, *14*, e0216349. [[CrossRef](#)]
37. Chen, Y.; Xu, Y.; Lin, Q.; Zhang, X. Model and criteria on the global finite-time synchronization of the chaotic gyrostat systems. *Math. Comput. Simul.* **2020**, *178*, 515–533. [[CrossRef](#)]
38. Izadbakhsh, A.; Nikdel, N. Chaos synchronization using differential equations as extended state observer. *Chaos Solitons Fractals* **2021**, *153*, 111433. [[CrossRef](#)]
39. Zhang, H.; Zhang, W.; Zhao, Y.; Ji, M.; Huang, L. Adaptive State Observers for Incrementally Quadratic Nonlinear Systems with Application to Chaos Synchronization. *Circuits Syst. Signal Process* **2020**, *39*, 1290–1306. [[CrossRef](#)]
40. Jahanzaib, L.S.; Trikha, P.; Matoog, R.T.; Muhammad, S.; Al-Ghamdi, A.; Higazy, M. Dual Penta-Compound Combination Anti-Synchronization with Analysis and Application to a Novel Fractional Chaotic System. *Fractal Fract.* **2021**, *5*, 264. [[CrossRef](#)]
41. Qi, F.; Qu, J.; Chai, Y.; Chen, L.; Lopes, A.M. Synchronization of Incommensurate Fractional-Order Chaotic Systems Based on Linear Feedback Control. *Fractal Fract.* **2022**, *6*, 221. [[CrossRef](#)]
42. Sabir, M.; Ahmad, S.; Marwan, M. Hopf bifurcation analysis for liquid-filled Gyrostat chaotic system and design of a novel technique to control slosh in spacecrafts. *Open Phys.* **2021**, *19*, 539–550. [[CrossRef](#)]
43. Marwan, M.; Abidin, M.Z.; Kalsoom, H.; Han, M. Generalized Full Order Observer Subject to Incremental Quadratic Constraint (IQC) for a Class of Fractional Order Chaotic Systems. *Fractal Fract.* **2022**, *6*, 189. [[CrossRef](#)]
44. Sprott, J.; Xiong, A. Classifying and quantifying basins of attraction. *Chaos Interdiscip. J. Nonlinear Sci.* **2015**, *25*, 083101. [[CrossRef](#)] [[PubMed](#)]
45. Wolf, A.; Swift, J.B.; Swinney, H.L.; Vastano, J.A. Determining Lyapunov exponents from a time series. *Phys. D Nonlinear Phenom.* **1985**, *16*, 285–317. [[CrossRef](#)]
46. Chlouverakis, K.E.; Sprott, J. A comparison of correlation and Lyapunov dimensions. *Phys. D Nonlinear Phenom.* **2005**, *200*, 156–164. [[CrossRef](#)]
47. Clemente-López, D.; Tlelo-Cuautle, E.; de la Fraga, L.G.; de Jesús Rangel-Magdaleno, J.; Muñoz-Pacheco, J.M. Poincaré maps for detecting chaos in fractional-order systems with hidden attractors for its Kaplan-Yorke dimension optimization. *AIMS Math.* **2022**, *7*, 5871–5894. [[CrossRef](#)]
48. Pecora, L.M.; Carroll, T.L. Synchronization in chaotic systems. *Phys. Rev. Lett.* **1990**, *64*, 821. [[CrossRef](#)]
49. Pecora, L.M.; Carroll, T.L. Driving systems with chaotic signals. *Phys. Rev. A* **1991**, *44*, 2374. [[CrossRef](#)]
50. Pecora, L.M.; Carroll, T.L. Master stability functions for synchronized coupled systems. *Int. J. Bifurc. Chaos* **1999**, *9*, 2315–2320. [[CrossRef](#)]
51. Slotine, J.J.E.; Li, W. *Applied Nonlinear Control*; Patient-Hall: Nottingham, MD, USA, 1991.